New Phytologist

Research

Accounting for landscape heterogeneity improves spatial predictions of tree vulnerability to drought

Amanda M. Schwantes[1], Anthony J. Parolari[2,3], Jennifer J. Swenson[1], Daniel M. Johnson[1,4], Jean-Christophe Domec[1,5], Robert B. Jackson[1,6], Norman Pelak[2,7] and Amilcare Porporato[2,7]

[1]Nicholas School of the Environment, Duke University, Box 90328, Durham, NC 27708, USA; [2]Department of Civil and Environmental Engineering, Duke University, Box 90287, Durham, NC 27708, USA; [3]Department of Civil, Construction, and Environmental Engineering, Marquette University, Milwaukee, WI 53233, USA; [4]Warnell School of Forestry and Natural Resources, University of Georgia, Athens, GA 30602, USA; [5]Bordeaux Sciences Agro, UMR INRA-ISPA 1391, 33195 Gradignan, France; [6]Department of Earth System Science, Woods Institute for the Environment and Precourt Institute for Energy, Stanford University, Y2E2 Building, 379B, Stanford, CA 94305, USA; [7]Department of Civil and Environmental Engineering and Princeton Environmental Institute, Princeton University, Princeton, NJ 08544, USA

Author for correspondence:
Amanda M. Schwantes
Tel: +1 571 344 2883
Email: amanda.schwantes@duke.edu

Received: *31 January 2018*
Accepted: *14 May 2018*

New Phytologist (2018)
doi: 10.1111/nph.15274

Key words: climate change, drought-induced tree mortality, heat load, landscape diversity, soil moisture, stochastic processes, topographic convergence, water stress.

Summary

- As climate change continues, forest vulnerability to droughts and heatwaves is increasing, but vulnerability varies regionally and locally through landscape position. Also, most models used in forecasting forest responses to heat and drought do not incorporate relevant spatial processes.
- In order to improve spatial predictions of tree vulnerability, we employed a nonlinear stochastic model of soil moisture dynamics accounting for landscape differences in aspect, topography and soils. Across a watershed in central Texas we modeled dynamic water stress for a dominant tree species, *Juniperus ashei*, and projected future dynamic water stress through the 21st century.
- Modeled dynamic water stress tracked spatial patterns of remotely sensed drought-induced canopy loss. Accuracy in predicting drought-impacted stands increased from 60%, accounting for spatially variable soil conditions, to 72% when also including lateral redistribution of water and radiation/temperature effects attributable to aspect. Our analysis also suggests that dynamic water stress will increase through the 21st century, with trees persisting at only selected microsites.
- Favorable microsites/refugia may exist across a landscape where trees can persist; however, if future droughts are too severe, the buffering capacity of an heterogeneous landscape could be overwhelmed. Incorporating spatial data will improve projections of future tree water stress and identification of potential resilient refugia.

Introduction

As climate change continues, more frequent and intense heatwaves and droughts will likely lead to greater tree mortality (Allen *et al.*, 2015). Instances of climate-induced tree mortality have already been documented world-wide (Allen *et al.*, 2010). Increases in tree die-off can alter plant community composition and species distributions (Mueller *et al.*, 2005; Engelbrecht *et al.*, 2007; Clark *et al.*, 2016), with consequences to biodiversity, carbon cycling, hydrology and biophysics (e.g. Ciais *et al.*, 2005; Jackson *et al.*, 2008; Vicente-Serrano *et al.*, 2014).

Empirical (e.g. bioclimate-envelope) or process-based models (e.g. Dynamic Global Vegetation Models, DGVMs) are two commonly used methods to predict how forests will respond to changes in climate. Spatial patterns of canopy loss often follow local stress gradients and depend on both climate and edaphic factors (Loehle & LeBlanc, 1996; Gitlin *et al.*, 2006; McLaughlin *et al.*, 2017). Although a few bioclimate-envelope models now account for topography (e.g. Lutz *et al.*, 2010), they lack mechanistic representations of tree mortality. Alternatively, DGVMs include various mechanisms for modeling tree mortality; however, their algorithms are rarely tested with spatially explicit canopy loss observations (McDowell *et al.*, 2011), and often do not account for landscape heterogeneity of abiotic factors at fine spatial resolutions, such as soil conditions, slope and aspect (Moorcroft, 2006), even though these data are readily available for many locations. Many studies have focused on improving model representations of the physiological mechanisms of tree mortality (McDowell *et al.*, 2013; Parolari *et al.*, 2014; Mackay *et al.*, 2015); however, only a few have examined if including landscape heterogeneity would improve predictions of tree mortality (Tague *et al.*, 2013; Anderegg *et al.*, 2015; Tai *et al.*, 2017).

Spatial patterns of tree mortality are associated with changes in soil texture and depth (Bowker *et al.*, 2012; Peterman & Waring,

2014; Twidwell *et al.*, 2014), topographic position (Adams *et al.*, 2014; Hawthorne & Miniat, 2017) and local water stress gradients (Gitlin *et al.*, 2006). Soil moisture variability across a landscape is driven by spatial variability in soil texture and depth to bedrock, surface runoff and subsurface lateral flow of water (Dunne *et al.*, 1975; Beven & Kirkby, 1979), and differences in radiation and resulting evaporation due to aspect and slope (Moore *et al.*, 1991; McCune & Keon, 2002). This landscape heterogeneity creates microsites or refugia with cooler, moister conditions that allow for tree survival during severe drought events. However, rarely is landscape heterogeneity considered in models, even though topography is important in identifying refugia locally buffered from climate change.

Many studies have found that the topographic wetness index (TWI) is significantly correlated to spatial patterns of soil moisture (Moore *et al.*, 1988; Western *et al.*, 1999) and tree mortality (Kaiser *et al.*, 2013). TWI is a spatial distribution function that can be used to describe lateral subsurface water flow along hillslopes (Beven, 1995). It is a physically based index of hydrological similarity, with areas having similar index values likely to respond in hydrologically similar ways (Beven, 1997). TWI is defined as $\log_e(a_c/\tan(b))$, where a_c is the upslope contributing area per unit contour length and $\tan(b)$ is the local land surface slope. The index assumes that the hydraulic gradient (i.e. a metric controlling the capacity of accumulated water to pass through the grid cell) is approximated by the local slope, and that lateral discharge (i.e. the water volume passing through a grid cell) is proportional to upslope contributing area (Quinn *et al.*, 1995; Beven, 1997).

Spatial patterns of soil moisture also are correlated with solar radiation (Western *et al.*, 1999) and landscape positions with higher insolation often have greater tree mortality (Kaiser *et al.*, 2013). In the northern hemisphere, south-facing slopes tend to have greater temperatures and evaporative demand, because they receive more radiation per unit area (i.e. insolation) compared to north-facing slopes. Additionally, although the amount of radiation is equivalent on eastern- and western-facing slopes averaged over a day, insolation on western-facing slopes is highest in the afternoon, leading to higher afternoon temperatures (McCune & Keon, 2002). Higher temperatures result in greater vapor-pressure deficits and potential evapotranspiration (PET). Under high temperatures and vapor-pressure deficits, trees typically close stomata, to reduce transpiration and protect the integrity of the plant hydraulic system by maintaining water potentials above irreversible embolism thresholds. In turn, this stomatal response, decreases photosynthesis.

In order to model plant–water relationships, two kinds of forest ecohydrological models exist: empirically-based models defining statistical relationships, but with little input of a system's structure; and process-based models defining key mechanisms to describe the structure and functioning of a system (Korzukhin *et al.*, 1996). Inevitably, there is a trade-off between purely empirical models, which can be biased when extrapolated beyond observed input values, and process-based models that can have higher error attributable to lack of data for parameters, especially at global scales (Adams *et al.*, 2013). However, these model classifications are not mutually exclusive. In the present study, we combine modeling frameworks by using a statistical–dynamic model of soil–plant water to model the probability of tree vulnerability to drought. Simplified mortality mechanisms are incorporated (Parolari *et al.*, 2014); the model is forced using stochastic precipitation (Laio *et al.*, 2001; Rodriguez-Iturbe & Porporato, 2004); and spatially explicit input parameters are included. The probability of tree mortality is then predicted given the mean intensity, duration and number of threshold crossings for percentage loss in hydraulic conductivity (PLC) associated with tree vulnerability to embolism curves. Simulations show, for instance, that tree species impacted by drought spend more time at higher PLC values (McDowell *et al.*, 2013; Adams *et al.*, 2017); chronically high PLC values among other risk factors also can predispose a tree to mortality (Sperry & Love, 2015).

From October 2010 to September 2011, Texas experienced its most severe one-year drought since record-keeping began in 1895 (Hoerling *et al.*, 2013). The drought killed millions of trees across the region (Moore *et al.*, 2016; Schwantes *et al.*, 2016, 2017). First, we combine a new modeling approach with species-specific physiological parameters and a detailed spatial dataset of tree canopy loss (Schwantes *et al.*, 2017; Johnson *et al.*, 2018a,b). Starting with a nonlinear stochastic model of plot-scale soil moisture dynamics for a single watershed in central Texas (Laio *et al.*, 2001), we integrate plant hydraulic thresholds and landscape processes, incorporating effects of lateral redistribution of water as well as radiation and temperature differences on dynamic soil moisture. Second, we explore the effect of incorporating landscape heterogeneity in models, when forecasting future drought stress, to understand whether landscape heterogeneity will buffer against future droughts projected in the 21st century. We use climate projections under multiple climate-warming trajectories and compare models with and without landscape heterogeneity.

Materials and Methods

Study area

Our study area is a watershed in the Edwards Plateau region of Texas (Fig. 1). We model tree water stress for a dominant tree species, *Juniperus ashei*. Our analysis only includes areas where *J. ashei* is a dominant species, as defined using an ecological systems map of Texas (Elliott *et al.*, 2014) and a percentage tree cover threshold > 25%, using the National Land Cover Database percentage tree cover product (Homer *et al.*, 2015). In 2011, a severe drought and heatwave led to 9.5% tree canopy loss overall across Texas, with *J. ashei* woodlands being one of the systems most impacted by the drought (Schwantes *et al.*, 2017), even though *J. ashei* is an extremely drought-tolerant species, with low vulnerability to root/stem embolism compared to other species in this region (Johnson *et al.*, 2018b). Within the study watershed, we acquired maps of drought-impacted area in 2011 from Schwantes *et al.* (2017), which were used to validate our tree water stress models.

Soil water balance model

Following Laio *et al.* (2001), we employ a nonlinear stochastic, ordinary differential equation of soil moisture dynamics, where rainfall follows a marked Poisson process interpreted on a daily timescale. We express the soil moisture (s) balance at a point as:

$$nZ_r \frac{ds(t)}{dt} = R(t) - I(t) - Q[s(t), t] - \mathrm{ET}[s(t)] - L[s(t)] \quad \text{Eqn 1}$$

(Z_r, active soil depth; n, porosity; $s(t)$, relative soil moisture content; $R(t)$, rainfall rate; $I(t)$, amount of rainfall intercepted by the canopy cover; $Q[s(t),t]$, surface/subsurface runoff rate; $\mathrm{ET}[s(t)]$, evapotranspiration rate; $L[s(t)]$, leakage below the root zone). The runoff, evapotranspiration and leakage rate depend on soil moisture levels through simple yet realistic representations of plant hydraulics, soil properties and topography. Under steady-state conditions, we obtain analytical solutions of the soil moisture probability density function for each 30-m grid cell across the watershed. The solution is provided in Supporting Information Eqn S1, Methods S1; however, the full derivation can be found in Laio *et al.* (2001) and Rodriguez-Iturbe *et al.* (1999). We then assess the role of climate, soil properties, plant hydraulics and topography on soil moisture dynamics and associated tree water stress, by adapting the framework for modeling dynamic water stress, originally proposed by Laio *et al.* (2001) and Porporato *et al.* (2001), Fig. 2.

Infiltration: rainfall, canopy interception and lateral water flow

Infiltration from rainfall is treated as an external random forcing factor where the occurrence of a rainfall event follows a marked Poisson process with a mean storm frequency, λ (d^{-1}). The depth of each rainfall event follows an exponential probability density function with a mean depth, α (cm), where α represents the amount of rainfall reaching the soil, while not accounting for canopy interception or lateral water flow. These distributions are commonly used to model rainfall at the daily timescale (Rodriguez-Iturbe *et al.*, 1999; Laio *et al.*, 2001; Porporato *et al.*, 2001; Parolari *et al.*, 2014). Following Daly *et al.* (2008), we assume that for small storm events below a certain threshold, Δ, the canopy completely intercepts all rainfall. For *J. ashei*, $\Delta = 0.25$ cm; storms below this value are typically fully intercepted (Owens *et al.*, 2006). The process describing the frequency of a rainfall event then becomes a censored marked Poisson process, and λ is reduced to λ' as:

$$\lambda' = \lambda e^{-\Delta/\alpha} \quad \text{Eqn 2}$$

For larger rainfall events above Δ, throughfall (e.g. precipitation minus interception) is linearly related to the depth of the rainfall event (Daly *et al.*, 2008). On average about 35% of bulk rainfall is intercepted by the canopy of *J. ashei* per storm event and sequentially lost due to evaporation (Owens *et al.*, 2006). The depth of each rainfall event still follows an exponential distribution; however, the mean rainfall depth is reduced to (k_i α), where $k_i = 0.65$ (Owens *et al.*, 2006).

In order to predict the pattern of soil moisture attributable to topographic position (e.g. describing lateral surface and subsurface flow from topographically divergent areas such as ridges to topographically convergent areas such as valleys), we further modify the mean rainfall depth (k_i α) to depend on each pixel's TWI, which is defined as:

$$\mathrm{TWI} = \log_e\left(\frac{a_c}{\tan(b) + 0.001}\right) \quad \text{Eqn 3}$$

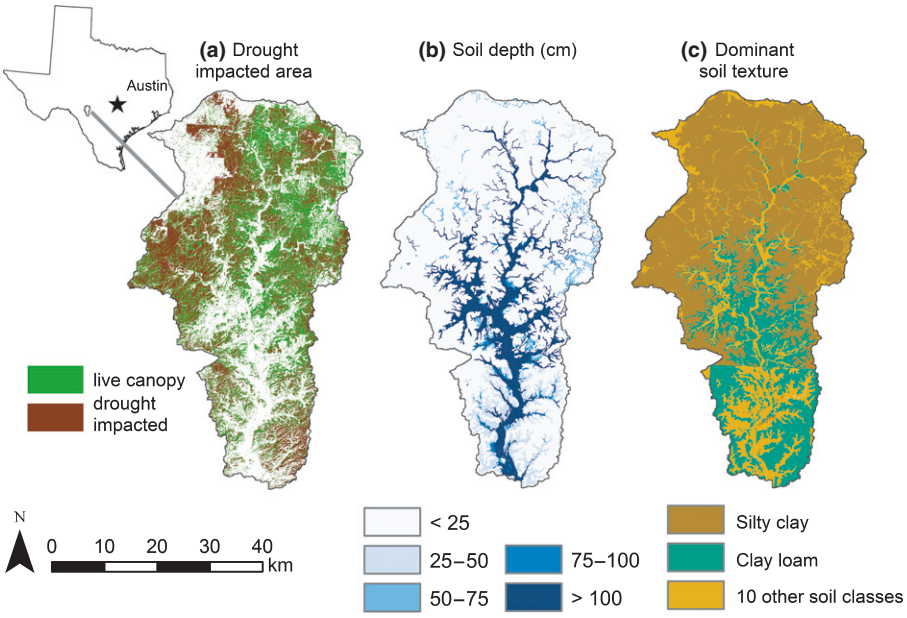

Fig. 1 Comparison of (a) drought-impacted area, defined as pixels with > 25% canopy loss acquired from Schwantes *et al.* (2017), (b) soil depth and (c) soil texture, both acquired from the SSURGO database (United States Department of Agriculture, 2014), for a watershed in the Edwards Plateau region of Texas.

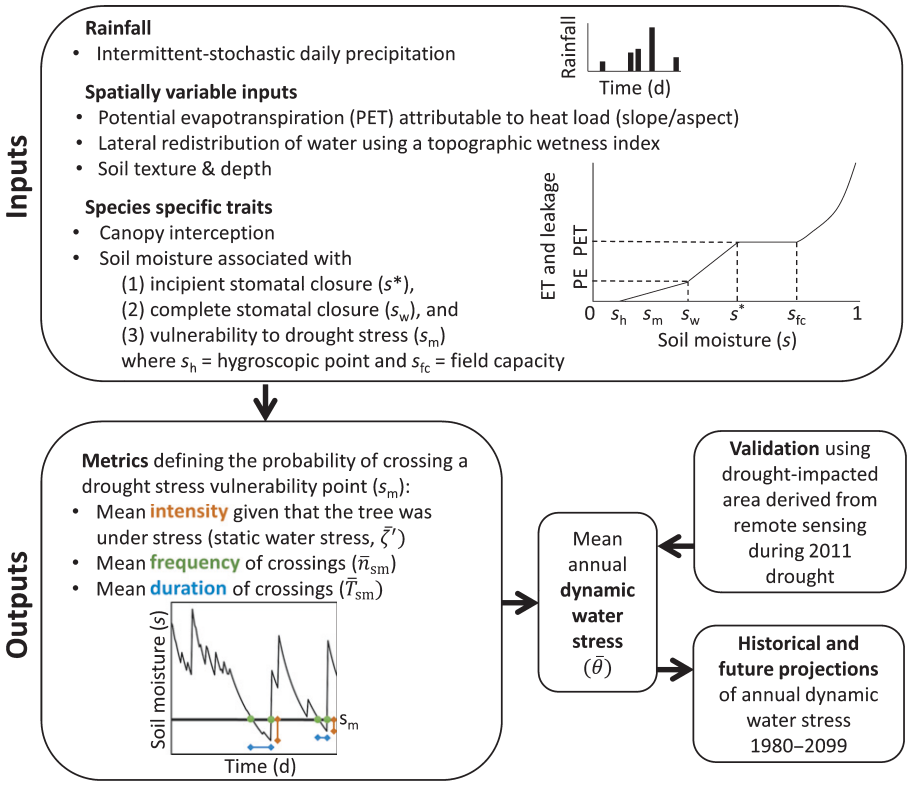

Fig. 2 Model overview: inputs include climate, tree physiology, soil and landscape parameters. Dynamic water stress incorporates outputs related to mean intensity, duration, and number of times a soil moisture threshold associated with severe drought-stress was crossed using a daily time-step and averaged over 1 yr. Remotely-sensed observations from 2011 are used to validate dynamic water stress. We then modeled annual dynamic water stress from 1980 to 2099.

(a_c, upslope contributing area (m^2); b, local slope angle (degrees) (Beven, 1997)). Upslope contributing areas range from 900 m^2 (e.g. the size of a single pixel) to the total area of the watershed (1961 km^2). To avoid undefined values of TWI in areas of zero local slope (i.e. a zero denominator), we add a small number (0.001) to the denominator for all pixels. TWI is calculated using a 30-m digital elevation model (DEM) from the Shuttle Radar Topography Mission (SRTM; v2). We calculate a_c using a multiple flow direction approach and the TauDEM ArcGIS toolbox (Tarboton, 2005).

Topographically convergent areas (e.g. valleys) tend to be associated with higher than average values of TWI, greater upslope contributing area (e.g. greater lateral discharge) and lower slopes (e.g. low hydraulic gradient). Therefore, the mean rainfall depth is adjusted for each pixel to account for landscape position, by redistributing water from areas of low TWI to areas of high TWI. Thus, we use the index to modify water inputs (α'), which now represent both infiltration from rainfall as well as lateral surface flow and subsurface lateral discharge. If soil moisture is rapidly redistributed daily during each individual storm event then α' can be reasonably linked to TWI as

$$\alpha' = k_i \times \alpha\left[1 + f \times \frac{[\mathrm{TWI} - \overline{\mathrm{TWI}}]}{\overline{\mathrm{TWI}}}\right] \qquad \text{Eqn 4}$$

(f, a parameter that controls the magnitude of lateral redistribution). A sensitivity analysis is performed using f from 0.1 to 1.0, in increments of 0.1.

Losses: evapotranspiration and leakage

Evapotranspiration, ET(s), accounts for losses from both soil evaporation $E(s)$ and tree transpiration $T(s)$. We assume that for this system, ET(s) has an upper limit defined by the potential evapotranspiration, PET, which depends on climate conditions and the tree species. We also assume that tree water uptake from the soil declines as a function of water stress. Under water stress, trees will partially close their stomata, and transpire at a reduced rate, up to a point where stomata close completely and transpiration ceases. Following (Laio *et al.*, 2001), we model this process by assuming that trees transpire at a maximum rate above a soil moisture associated with a stress point (s^*). When soil moisture drops below s^*, transpiration decreases linearly up to a soil moisture associated with complete stomatal closure (s_w). Below s_w only soil evaporation occurs, which we model as decreasing linearly from potential soil evaporation, PE, at s_w to zero at the hygroscopic point, s_h, defined as follows:

$$\mathrm{ET(s)} = \begin{cases} \mathrm{PE}' \frac{s - s_h}{s_w - s_h}, & s_h < s \le s_w, \\ \mathrm{PE}' + (\mathrm{PET}' - \mathrm{PE}') \frac{s - s_w}{s^* - s_w}, & s_w < s \le s^*, \\ \mathrm{PET}', & s^* < s \le 1, \end{cases} \qquad \text{Eqn 5}$$

Evapotranspiration also depends on the surface energy budget (Moore *et al.*, 1991). We account for spatial variation in PET, defined as:

$$\mathrm{PET}' = \mathrm{PET} \times \mathrm{HL} \qquad \text{Eqn 6}$$

by using a heat load index (HL), which accounts for potential direct incident radiation and temperature differences attributable to aspect and steepness of slope (McCune & Keon, 2002; Evans *et al.*, 2014). Higher values of PET′ are associated with greater radiation (e.g. south-facing slopes) and warmer afternoon temperatures (e.g. western-facing slopes).

In order to differentiate potential soil evaporation (PE) from potential transpiration, we use the fraction of solar radiation that the canopy intercepts, defined as:

$$v_f = 1 - e^{-k_f \times \mathrm{LAI}} \qquad \text{Eqn 7}$$

where LAI represents leaf area index and k_f is a light extinction coefficient (Landsberg, 1986; Norman & Campbell, 1989). The higher this vegetation factor (v_f), the less PET is partitioned into PE, following:

$$\mathrm{PE}' = \mathrm{PET}' \times (1 - v_f) \qquad (8)$$

We measured LAI using a LAI-2200C Plant Canopy Analyzer (Li-Cor, Lincoln, NE, USA) during July 2016 at Colorado Bend State Park, in Central Texas. All measurements were taken at twilight, to minimize changing sky-conditions and scattering errors. We used a 45° view cap and masked out the outermost ring. Measurements were taken every 1 m, along 10 transects, each 10 m in length. The average LAI for stands of *J. ashei* was 2.92 ± 0.46 ($\pm$ SD). We used a k_f for juniper of 0.37 from Kiniry (1998).

The soil moisture value at which stomata start to close (s^*), and the soil moisture at which stomata close completely (s_w), both depend on tree species and soil texture. We obtain the relative soil moisture, s, for a corresponding soil water potential, Ψ_s, using soil water retention curves, as defined in Clapp & Hornberger (1978), as follows:

$$\Psi_s = \bar{\Psi}_s s^{-b} \qquad \text{Eqn 9}$$

($\bar{\Psi}_s$ and b, experimentally derived parameters that vary with soil texture). The relative soil moisture for the hygroscopic point, s_h, and the field capacity, s_{fc}, can be found using Eqn 9 and the following respective soil water potentials: $\Psi_{sh} = -10$ MPa (Laio *et al.*, 2001) and $\Psi_{sfc} = -0.033$ MPa (Hudson, 1994). To define Ψ_{s*} we assume that stomata start to close when the soil water potential reaches a point associated with 12% loss of hydraulic conductance in the leaves, P_{12}, -1.0 MPa for *J. ashei* (Johnson *et al.*, 2016). We used the P_{12}, or air-entry point, because it represents the point on a leaf hydraulic vulnerability curve (see Fig. 3b) where loss of conductance increases substantially (Domec & Gartner, 2001). We define Ψ_{sw} by assuming that stomata close completely when the soil water potential reaches the turgor loss point, TLP, for *J. ashei*, which is -3.8 MPa (Johnson *et al.*, 2018a). This TLP is associated with a 99.8% loss of leaf hydraulic conductance (see Fig. 3b). Also, s^* and s_w represent the soil moisture associated with the start of stomatal conductance reduction and near-zero stomatal conductance, respectively (Fig. 3a) using data from Johnson *et al.* (2018b), and described further in Methods S2 and Table S1.

Soil properties were obtained from the Soil Survey Geographic (SSURGO) database (United States Department of Agriculture 2014). We computed area- and depth-weighted averages of percentage sand, clay and silt for each soil polygon, whereas soil depth (Z_r) was acquired directly. Based on these soil texture observations, we classified each soil polygon as one of 12 United States Department of Agriculture (USDA) soil classes. The experimentally derived parameters for the soil water retention curves, $\bar{\Psi}_s$ and b, the saturated hydraulic conductivity, K_s, and the porosity, n, were estimated using the USDA soil type classifications, following Clapp & Hornberger (1978), Daly *et al.* (2004) and

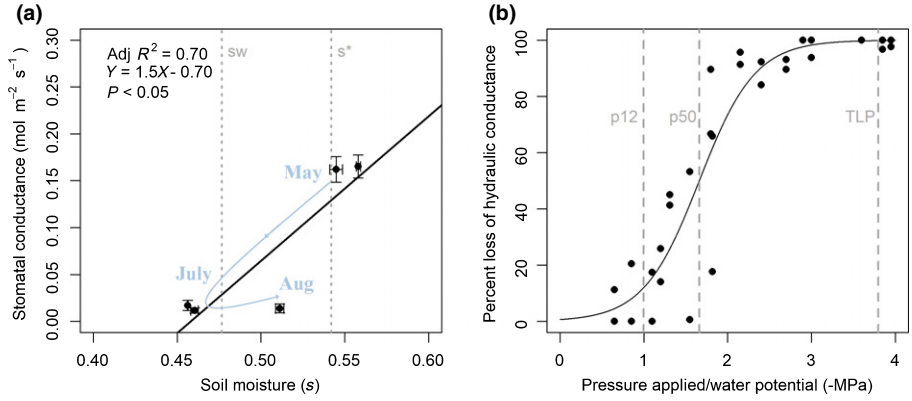

Fig. 3 Justification for selecting parameters associated with incipient and complete stomatal closure: (a) Field observations of average stomatal conductance for *Juniperus ashei* as a function of soil moisture, where soil moisture for a silty clay was derived by assuming that measured pre-dawn leaf water potential was equivalent to soil water potential. These field measurements for 5 d in summer 2013 were taken for *J. ashei* in central Texas by Johnson *et al.* (2018b). Each point represents a daily average; error bars represent standard errors associated with variability between individuals and time of day; and the blue line shows the lagged recovery following a time-period of near zero stomatal conductance observed in July, despite rain returning in August (Johnson *et al.*, 2018b). (b) Percentage loss of leaf hydraulic conductivity in *J. ashei*. The P_{12} or air entry point was chosen for the incipient stomatal closure point (s^*). The turgor loss point (TLP) was chosen to represent complete stomatal closure (s_w). Data reproduced with permission from Johnson *et al.* (2016).

Laio *et al.* (2001). Lastly, we assume that the soil hydraulic conductivity, $K(s)$, follows an exponential decay from K_s, at $s = 1$ to zero, at $s = s_{fc}$:

$$K(s) = L(s) = \frac{K_s}{e^{\beta(1-s_{fc})} - 1}\left[e^{\beta(s-s_{fc})} - 1\right], \quad s_{fc} < s \leq 1 \qquad \text{Eqn 10}$$

where β depends on the soil texture and is equal to $2b + 4$ and b is defined in Eqn 9 (Laio *et al.*, 2001).

Static and dynamic water stress

Our objective was to model tree water stress in a semi-arid ecosystem and evaluate factors contributing to tree mortality. Although some isohydric species tend to have greater mortality following periods of near-zero gas exchange, *Juniperus* mortality likely occurs with hydraulic failure, especially in the absence of pathogens (Plaut *et al.*, 2012); therefore, we define a new soil moisture level below the point of near-zero gas exchange, at which a tree is under severe stress and vulnerable to mortality, s_m. We define Ψ_{sm} as the soil water potential associated with a 50% loss in hydraulic conductivity in the roots, root P_{50}, which is −9.5 MPa for *J. ashei* (Johnson *et al.*, 2016). Brodribb *et al.* (2010) found that stem P_{50} correlated with lethal water potential thresholds across four conifer species. Instead of using stem P_{50}, we used the root P_{50} as Ψ_{sm}, because roots are often more vulnerable to cavitation compared to shoots, especially in conifers (Kavanagh *et al.*, 1999). Moreover, the root P_{50} acquired from Johnson *et al.* (2016) was nearly identical to modeled critical soil water potential, representing the point to which *J. ashei* could no longer transport water, as modeled by Johnson *et al.* (2018b) using the Terrestrial Regional Ecosystem Exchange Simulator model (Sperry *et al.*, 1998; Mackay *et al.*, 2015). The stem P_{50}, −13.1 MPa, (Willson *et al.*, 2008), and root P_{50}, −9.5 MPa, are much lower than the leaf P_{50} of −1.66 MPa (Johnson *et al.*, 2018b), likely due to the hydraulic vulnerability segmentation hypothesis, which suggests that distal portions (e.g. leaves) will embolize first at less negative pressures to avoid hydraulic impairment in the stems/roots (Tyree & Ewers, 1991; Johnson *et al.*, 2016).

We adapt the static water stress equations developed by Porporato *et al.* (2001), and define static water stress, ζ, as zero at $s > s_m$ to approaching 1 as s approaches the hygroscopic point, s_h:

$$\zeta(t) = \left[\frac{s_m - s(t)}{s_m - s_h}\right], \quad s_h < s(t) \leq s_m \qquad \text{Eqn 11}$$

We expect that larger deviations from s_m would result in higher probabilities of tree mortality. Derivations for computing the probability distribution for the static water stress, ζ (Eqn S3), as well as the mean static water stress, $\bar{\zeta}$ (Eqn S6), and the mean static water stress given that the tree was under stress, $\bar{\zeta}'$ (Eqn S7), can be found in the Supporting Information.

In order to predict tree vulnerability to drought-induced tree mortality, we calculate the dynamic water stress $\bar{\theta}$ as follows:

$$\bar{\theta} = \begin{cases} \left(\frac{\bar{\zeta}'\bar{T}_{sm}}{T_{seas}}\right)^{1/\sqrt{\bar{n}_{sm}}} & \text{if } \bar{\zeta}'\bar{T}_{sm} < \bar{T}_{seas} \\ 1 & \text{otherwise,} \end{cases} \qquad \text{Eqn 12}$$

$\bar{\theta}$ was adapted from the original equation proposed by Porporato *et al.* (2001) by incorporating $\bar{\zeta}'$ and two crossing properties below the soil moisture threshold associated with severe water stress and potential mortality, s_m. The two crossing properties include: $\bar{n}_{sm}$ the average number of crossings below s_m, and $\bar{T}_{sm}$ the average time spent below s_m. As such, dynamic water stress incorporates mean intensity, duration and frequency of soil water deficits associated with crossings below root P_{50}. We can obtain analytical solutions for both $\bar{T}_{sm}$ and $\bar{n}_{sm}$. Full solutions are in the Supporting Information, Eqns S8 and S9, respectively. We used the full year as the duration of the growing season (T_{seas}), because *J. ashei* is an evergreen species, and the model was run at a 30-m spatial resolution.

Historical and future projections of water stress

Historical, 1980–2015, spatially interpolated 4-km gridded daily precipitation and monthly potential evapotranspiration calculated using Penman–Monteith for a grass reference surface, PET_g, were acquired from gridMET (Abatzoglou, 2013). We used spatial averages across the watershed for annual PET_g, the mean rainfall depth, α, and the average time between rainfall events, $1/\lambda$. For a similar juniper-dominated woodland/savannah in the Edwards Plateau of Texas, Heilman *et al.* (2014) found an average annual PET of 69 cm from 2005 to 2009, whereas PET_g estimates in this region were 176 cm according to gridMET; therefore, we applied a plant correction coefficient of 0.39. This value was similar to expected crop coefficients for trees, which range from 0.4 to 1.0 (Allen *et al.*, 1998). The PET for *J. ashei* was calculated by multiplying the crop coefficient, 0.39, by PET_g acquired from gridMET (Abatzoglou, 2013).

We also acquired downscaled (4-km) climate projections from the coupled model intercomparison project, CMIP5, under two representative concentration pathways, RCP, 4.5 and 8.5 trajectories from 2006 to 2099 for PET_g and precipitation (Abatzoglou & Brown, 2012). Of 20 global climate models (GCMs) that we considered, we selected 10 GCMs that showed the best performance in projecting historical annual precipitation values (1980–2005) for our study watershed, considering mean absolute error (MAE) in annual precipitation. We again took spatial averages across the watershed for future annual projections of PET_g, α and λ. We then examined historical (1980–2015) and future projections of dynamic water stress (2006–2099) for models with and without landscape heterogeneity.

Accuracy assessments

The soil water balance model was run for each 30-m grid cell within the watershed, to obtain spatially explicit estimates of tree water stress. We then compared our modeled results forced using PET, α and λ values for 2011 to remotely sensed 30-m drought-impacted area maps for 2011 from Schwantes *et al.* (2017), where

areas of drought-impact were defined as having > 25% canopy loss. We first aggregated both modeled results and observations of drought-impacted area to hydrologically similar but noncontiguous stands of *J. ashei*, similar to Tai *et al.* (2017). Hydrologically similar stands, $n = 24$, were defined as stands with similar aspects, NE, −45° to 135° vs SW, 135° to 315°; soil depths, < 100 cm vs > 100 cm; soil texture, silty clay, clay loam or other; and topographic divergence vs convergence, TWI below or above the mean, respectively. Following aggregation, we used linear regressions to compare modeled outputs to observations of drought-impacted areas.

We also identified stands of spatially contiguous pixels of two classes: drought-impacted vs homogenous live canopy. Pixels were considered contiguous if one of eight neighboring cells was the same class. We then compared explanatory power (e.g. Cragg and Uhler's pseudo R^2) for logistic regressions in predicting whether a stand was either drought-impacted or homogenous live canopy, using dynamic water stress as the continuous predictor variable. Dynamic water stress represents a probability of tree vulnerability to drought. Therefore, in order to select a threshold of dynamic water stress that best distinguished drought-impacted stands from live canopy stands, we used receiver operating characteristic (ROC) curves (Sing *et al.*, 2005). For multiple cut-off values of modeled dynamic water stress, ROC curves plot true positive rate (TPR, accurately predicting a drought-impacted stand) against true negative rate (TNR, accurately predicting a homogenous live canopy stand). The cut-off value that balanced TPR and TNR was chosen, using 10-fold cross-validation. To test whether accuracy improved when considering average dynamic water stress in larger stands, we sequentially removed stands below a certain size threshold. Other studies have found that aggregation up to a 100-m pixel (i.e. 1 ha) was necessary to improve correlations between modeled and observed soil moisture (Pellenq *et al.*, 2003). The water stress model was solved using MATLAB; statistical analysis was conducted in R; and spatial analysis was performed using ARCGIS and PYTHON.

Results

Comparing modeled water stress to observations of drought-impacted area

Using our dynamic water stress model for each 30-m pixel across a watershed in central Texas, we found that canopy loss from drought was greatest in areas of shallow soils, on hillslopes with low values of TWI, and on southwestern-facing aspects (Fig. 4). We started with models that only had spatially explicit soil conditions, and then added parameters associated with lateral

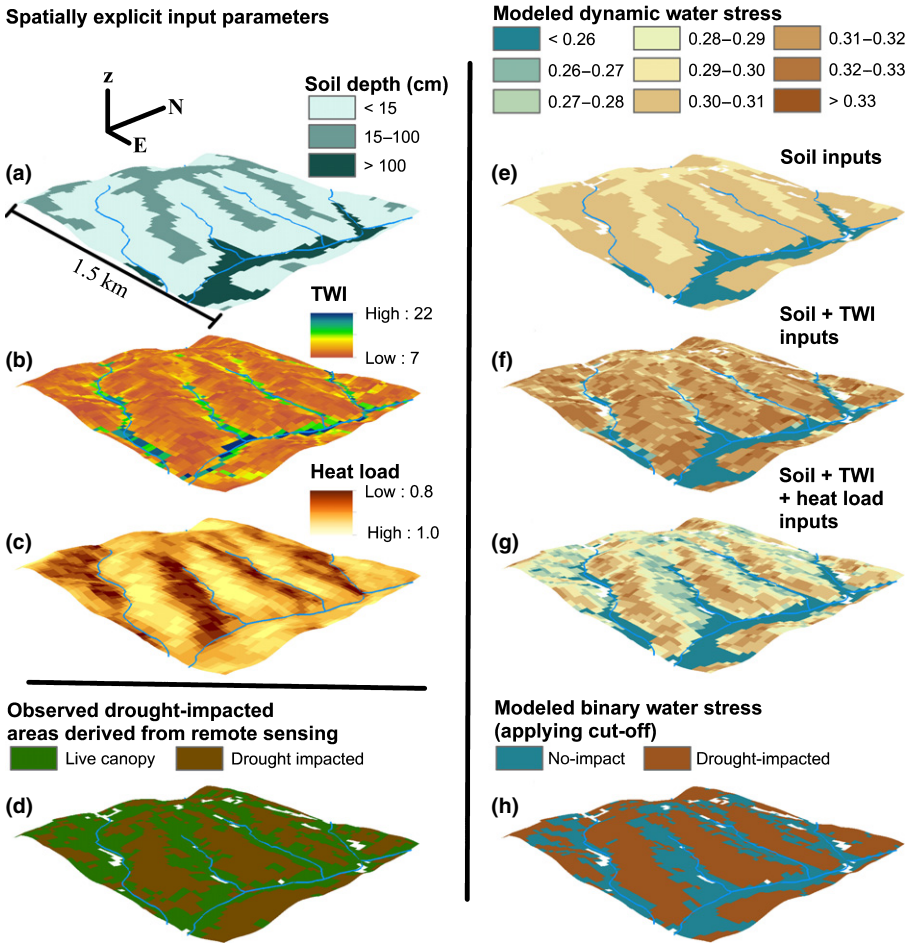

Fig. 4 Comparison of spatially explicit input variables of (a) soil depth, (b) topographic wetness index (TWI) and (c) heat load index to (d) a 30-m remotely sensed drought-impacted area map. We also present modeled estimates of mean dynamic water stress for scenarios including processes specific to (e) heterogeneous soil inputs, (f) lateral redistribution of water using TWI ($f = 1$) and (g) spatially variable potential evapotranspiration using a heat load index, accounting for radiation and temperature differences attributable to aspect. Using a cut-off value of dynamic water stress (defined in Table 2), we also show a binary water stress map (h), which is directly comparable to observed canopy loss (d).

redistribution and then spatially explicit PET driven by radiation and temperature differences attributable to aspect. Spatially distributed inputs, characterizing soil conditions, lateral water flow, and PET, all drove patterns of dynamic water stress across the landscape. By increasing model complexity, modeled dynamic water stress had higher spatial concordance with remotely-sensed observations of drought-impacted area (Fig. 4).

Modeled dynamic water stress varied across two important environmental gradients. As expected, dynamic water stress decreased with increasing soil depth, as simulated with the following assumptions: constant clay loam soil texture, constant PET and no lateral flow of water (Fig. 5a). Directly matching model predictions, observations of drought-impacted area also decreased with increasing soil depth. Furthermore, dynamic water stress decreased with increasing values of TWI (Fig. 5b). The model was forced using a constant clay loam soil texture and average soil depth. Observations of drought-impacted area aggregated up to 2-unit bins of TWI, also decreased with increasing TWI, following modeled dynamic water stress.

In order to test the accuracy in predicting observed values of canopy loss during the 2011 drought year, we first aggregated modeled results and observed drought-impacted area in 24 hydrologically similar but noncontiguous stands (Table 1). We compared explanatory power for linear regressions of observations of percentage drought-impacted area and four modeled outputs. We found that the explanatory power for dynamic water stress increased, as model complexity increased. When only considering spatial variability of soils, adjusted R^2 was equal to 0.76; however, when including lateral flow of water and spatially variable PET from radiation and temperature differences, the explanatory power increased to 0.82 (Table 1).

Second, we tested how well modeled dynamic water stress differentiated spatially contiguous *J. ashei* drought-impacted stands compared with homogenous live canopy stands. We compared Cragg and Uhler's pseudo R^2 for logistic regressions and percentage accuracy for a threshold distinguishing the two types of stands using ROC curves (Fig. 6; Table 2). We also tested the

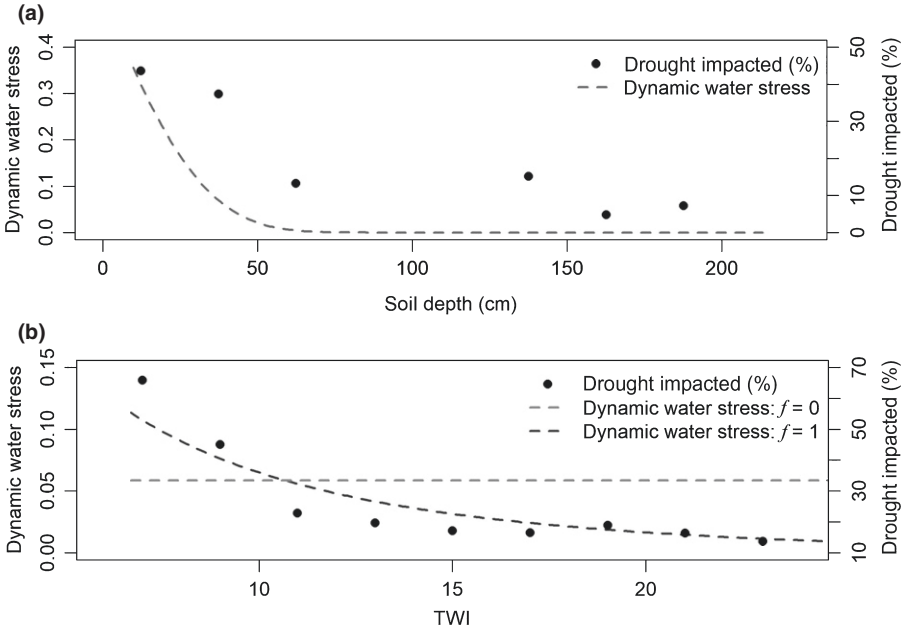

Fig. 5 Modeled dynamic water stress decreased with increasing (a) soil depth and no lateral redistribution ($f = 0$) and (b) topographic wetness index (TWI, forced with average soil depth and a clay loam soil texture). Modeled results tracked observed drought impacted area (right axis, black circles): in (a) the drought-impacted area was aggregated to noncontiguous stands with similar soil properties (e.g. clay loam soil texture with multiple soil depth bins of 25 cm) and in (b) the drought-impacted area was binned by two units of TWI for areas with clay loam soils.

Table 1 Summary of linear regression coefficients: a comparison of drought-impacted area to model outputs forced with the climate anomalies observed in 2011: dynamic water stress ($\bar{\theta}$), static water stress given that a tree was under stress ($\bar{\zeta}'$), the average number of crossings ($\bar{n}_{sm}$) below root P_{50} (50% hydraulic conductivity lost), and the average time spent ($\bar{T}_{sm}$) below root P_{50}, where $f = 1$, and the number of hydrologically similar noncontiguous stands is equal to 24

	Soils			Soils + LR			Soils + LR + H		
Modeled output	R^2	β	P	R^2	β	P	R^2	β	P
$\bar{\theta}$	0.76	0.90	***	0.80	0.93	***	0.82	1.02	***
$\bar{\zeta}'$,	0.75	0.52	***	0.75	0.52	***	0.76	0.53	***
$\bar{n}_{sm}$	0.77	0.02	***	0.83	0.02	***	0.85	0.03	***
$\bar{T}_{sm}$	0.75	−0.48	***	0.47	−0.37	***	0.45	−0.41	***

***, $P < 0.001$; Soils, soil texture and depth; LR, lateral redistribution; H, heat load.

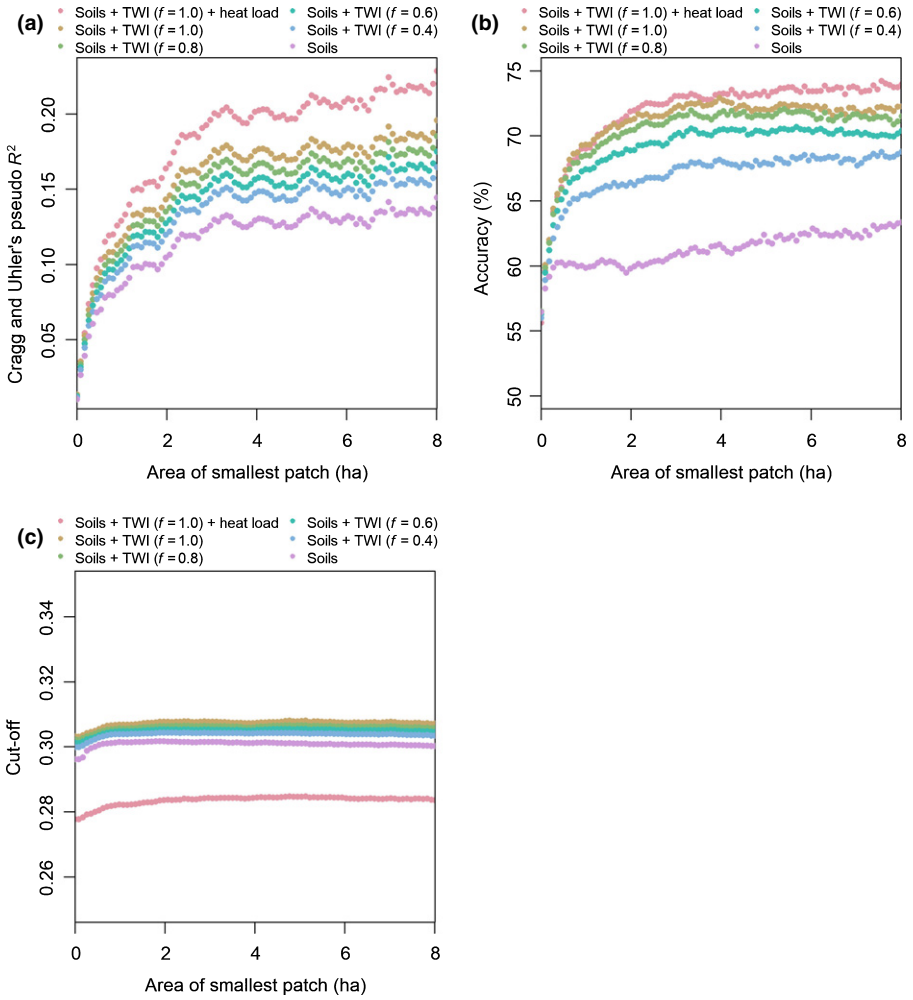

Fig. 6 Accuracy in distinguishing drought-impacted stands from homogenous live canopy stands of *Juniperus ashei* above a certain patch area threshold (*x*-axis): (a) Cragg and Uhler's pseudo R^2 for logistic regressions, (b) percentage accuracy and (c) the dynamic water stress cut-off defined using receiver operating characteristic (ROC) curves. Each line represents a different model with multiple levels of complexity, including only spatially variable soil conditions (soils), lateral redistribution of water (soils + topographic wetness index (TWI)) with the constant, *f*, ranging from 0.4, 0.6, 0.8 and 1.0, and spatially variable potential evapotranspiration (PET) due to radiation/temperature differences (soils + TWI + heat load). The number of stands ranged from *c.* 42 000 when including all size patches to *c.* 1000 when including only patches > 8 ha.

influence of only including stands above a certain stand size class. There seemed to be an inflection point, where percentage accuracy and explanatory power increased dramatically for stands >1 ha and started to level off at around 2 ha (Fig. 6). Also, increasing model complexity resulted in higher accuracy and higher explanatory power. For example, models that only included spatially variable soil conditions reached an accuracy of 60%, when considering stands >2 ha; however, when including spatially variable inputs related to soil, lateral flow of water and radiation/temperature effects, the accuracy increased to 72% (Table 2). Furthermore, increasing the amount of lateral redistribution of water, by increasing *f*, led to improvements in model accuracy and higher explanatory power. However, as *f* got larger and approached 1, large changes in *f* only led to minimal improvements in accuracy (Fig. 6). A cut-off value of 0.28 for dynamic water stress was most successful at distinguishing homogenous live canopy stands from drought-impacted stands (Table 2). We therefore used this cut-off value and $f = 1$, to determine the percentage of the landscape that surpassed a dynamic water stress value associated with canopy loss for both historical and future climate projections. The cut-off value was not dependent on the size of stands considered (Fig. 6c).

Projecting dynamic water stress through the 21st century

In order to understand how dynamic water stress is projected to change in the future, we selected 10 GCMs that showed the lowest MAE in predicting mean annual precipitation (Table S2). For several years in the 21st century and across several of the GCMs, the mean rainfall depth, α, and the time between rainfall events, $1/\lambda$, surpassed drought conditions that were more severe than the 2011 drought year (Fig. 7a,b). PET for *J. ashei* increased dramatically compared to historical averages for both RCP 4.5 and even more so for RCP 8.5 (Fig. 7c). Ensemble means of dynamic water stress across 10 GCMs showed that average dynamic water stress increased over the 21st century (Fig. 8a) for both RCP 4.5 and 8.5 scenarios. Furthermore, the percentage of the landscape surpassing a threshold of dynamic water stress associated with mortality increased through the 21st century (Fig. 8b). For models forced using no landscape heterogeneity, the maximum percentage of the area impacted by model construction was 100% for the most severe droughts projected in the 21st century. However, when landscape heterogeneity was included, the maximum percentage area impacted in the future was *c.* 90% for both RCP 4.5 and 8.5 (Table 3).

Table 2 Summary of logistic regression coefficients and outputs of the receiver operating characteristic (ROC) curve analysis for models of increasing complexity, testing the capacity of model outputs in distinguishing drought-impacted stands from homogenous live canopy stands

	Soils				Soils + LR				Soils + LR + H				
Model output	R^2	P	AIC	% acc	R^2	P	AIC	% acc	R^2	P	AIC	% acc	Cut-off
>1 ha													
$\bar{\theta}$	0.08	***	7715	60	0.12	***	7567	69	0.13	***	7502	69	0.28
$\bar{\zeta}'$,	0.08	***	7717	60	0.09	***	7711	60	0.09	***	7686	62	0.68
$\bar{n}_{sm}$	0.08	***	7718	59	0.13	***	7503	70	0.14	***	7428	69	10.35
$\bar{T}_{sm}$	0.08	***	7722	40	0.01	***	8054	59	0.01	***	8070	59	9.43
>2 ha													
$\bar{\theta}$	0.10	***	4570	60	0.14	***	4458	71	0.16	***	4396	72	0.28
$\bar{\zeta}'$,	0.10	***	4574	60	0.10	***	4569	60	0.11	***	4545	64	0.68
$\bar{n}_{sm}$	0.10	***	4573	59	0.16	***	4413	71	0.18	***	4340	72	10.43
$\bar{T}_{sm}$	0.10	***	4577	40	0.01	***	4822	59	0.01	***	4834	59	9.43

Model outputs included dynamic water stress ($\bar{\theta}$), static water stress given a tree was under stress ($\bar{\zeta}'$), the average number of crossings ($\bar{n}_{sm}$) below root P_{50} (50% hydraulic conductivity lost), and the average time spent ($\bar{T}_{sm}$) below root P_{50}, where $f = 1$, and the size of drought-impacted or homogenous live canopy stands of *J. ashei* was either > 1 ha or > 2 ha. ***, $P < 0.001$; Soils, soil texture and depth; LR, lateral redistribution using topographic wetness index (TWI); H, heat load. R^2, Cragg and Uhler's pseudo R^2; % acc, percentage accuracy in differentiating drought-impacted vs live canopy stands using ROC curve analysis and 10-fold cross-validation.

Discussion

Incorporating topography in models of tree water stress

Model estimates of dynamic water stress compared well with remotely-sensed observations of drought-impacted area from the 2011 drought. When using dynamic water stress to distinguish between drought-impacted stands vs homogenous live canopy stands > 2 ha, we found that accuracy increased from 60% for models including only spatially variable soil conditions to 72% for models considering soils and topography, including lateral redistribution of water using a topographic wetness index (TWI) and spatially variable potential evapotranspiration (PET) attributable to radiation/temperature differences (Table 2). Tai *et al.* (2017) also found that including topography to approximate lateral redistribution improved predictions of Aspen, *Populus tremuloides*, mortality in Colorado. Our approach expands upon Tai *et al.* (2017), by providing an alternative framework that cohesively integrates plant physiological thresholds limiting hydraulic capacity (Fig. 3b) and landscape processes. In the absence of widespread observations of leaf water potential thresholds for tree vulnerability to drying soil, the prediction of large-scale response to drought seems difficult. Our model requires simple physiological traits that are consistent with known mechanisms of plant hydraulic failure and that are routinely measured when investigating plant response to drought (e.g. air entry, 50% loss in hydraulic conductivity in the roots (root P_{50}) and turgor loss points derived from cavitation and pressure–volume curves, respectively).

When aggregating modeled results to larger stands (> 1 ha; Fig. 6), we observed improved accuracy, which could be attributable to hydrological processes acting across pixels. The topographic index, TWI, was used to directly relate the land surface to lateral water flow; however, the land surface may not be the best predictor of belowground processes. As an example, variations in the water table depth could be lower compared to variations in the land surface elevation (Wolock & Price, 1994). Also, the minimum size map delineation for the SSURGO soil database ranges from 0.4 to 4 ha; a much coarser resolution than the 30-m digital elevation maps used to derive TWI. Moreover, soil maps often show sharp, unrealistic changes of soil texture and soil depth between neighboring soil polygons (Zhu & Mackay, 2001); aggregating across stands may smooth these transitions. Lastly, at fine spatial scales, tree mortality could appear stochastic due to a variety of mechanisms that are not included in most models (e.g. insects and pathogens, harvesting/land management and plasticity of plant traits). For these reasons, accuracy improved as we aggregated modeled results to larger stands, until a threshold of *c.* 2 ha was reached. Past this threshold of 2 ha and up to 8 ha, accuracy did not increase substantially (Figs S1, 6).

Limitations

The modeling framework had a few important limitations. *Juniperus ashei* is an evergreen species; therefore, we defined the growing season as the full year, but did not include seasonal differences when modeling rainfall stochastically. Incorporating seasonality could improve our ability to model tree water stress (Viola *et al.*, 2008; Feng *et al.*, 2017). We did not consider water inputs from the deep regolith, which could provide additional sources of water (Fellows & Goulden, 2013). A few *J. ashei* individuals have been observed to access water in caves up to 8-m below the soil surface in central Texas (Jackson *et al.*, 1999). When examining tree water stress in the future, we did not consider effects associated with increased water use efficiency (WUE) from elevated atmospheric CO_2 concentrations. However, an experiment examining the interactive effects between elevated CO_2 and drought found that elevated CO_2 did not delay time to mortality for two gymnosperm species (Duan *et al.*, 2015). If

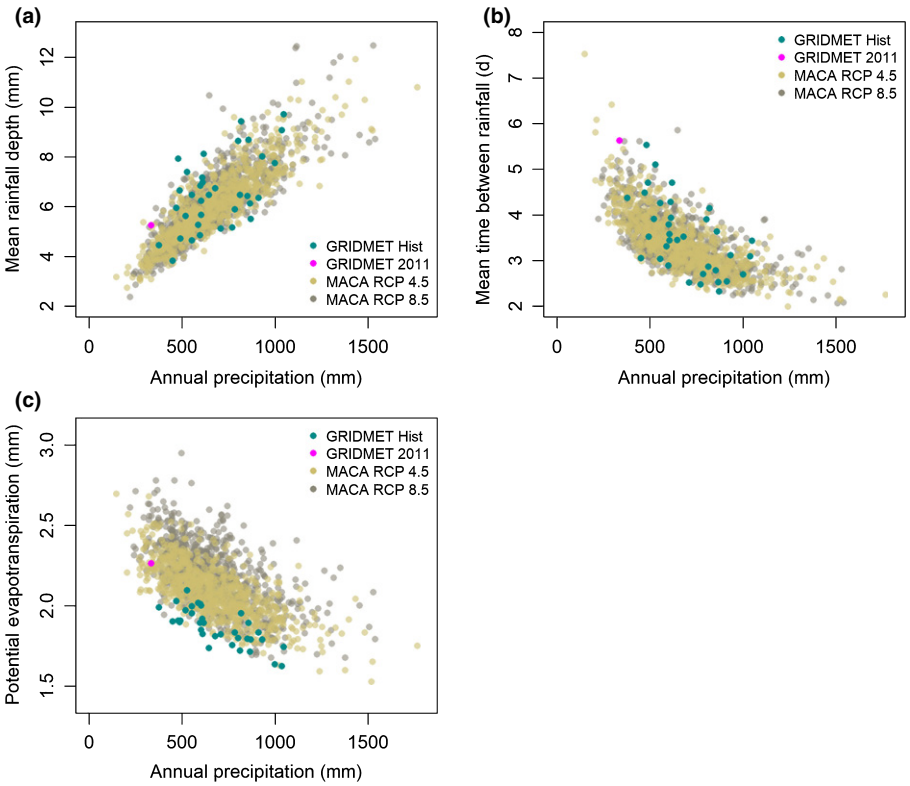

Fig. 7 Comparison of how climate parameters vary with annual precipitation: (a) α, mean rainfall depth (mm), (b) $1/\lambda$, time (days) between rainfall events, and (c) potential evapotranspiration (PET) for *Juniperus ashei*, using spatial averages across all areas in the watershed. We include both historical gridMET climate data: 1980–2015 (Abatzoglou, 2013) and future MACA climate projections: 2020–2099, from two representative concentration pathway trajectories, RCP 4.5 and 8.5, acquired from Abatzoglou & Brown (2012). Each point represents climate parameters for each year from 2020 to 2099, for each of the 10 global climate models (GCMs).

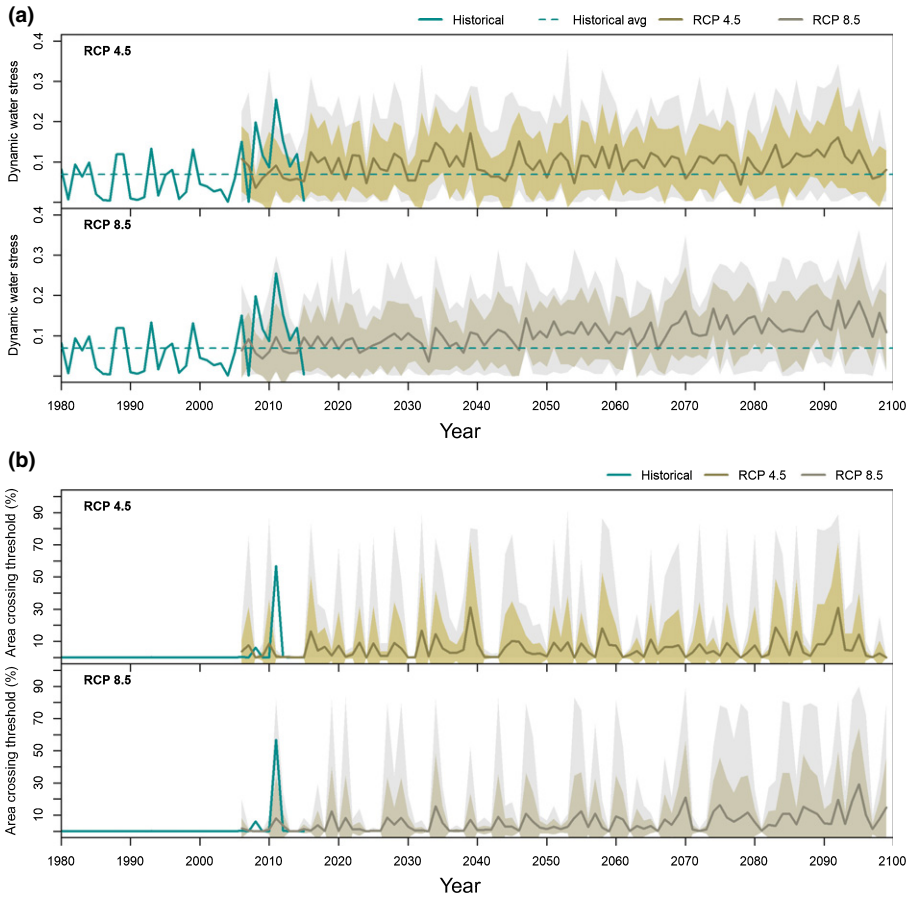

Fig. 8 Comparison of how dynamic water stress has changed over the past 35 yr (1980–2015) (Abatzoglou, 2013) and was projected to change in the future 2006–2099, using climate data from two representative concentration pathway trajectories, RCP 4.5 and 8.5 (Abatzoglou & Brown, 2012): (a) spatial averages of dynamic water stress across the watershed with *Juniperus ashei* cover and (b) percentage area drought-impacted (e.g. percentage of the landscape that surpassed the dynamic water stress threshold of 0.28 associated with canopy loss during the 2011 drought year, defined in Table 2). The dark line represents the average of 10 global climate models (GCMs), the colored shading: the standard deviation, and the gray shading: the range.

Table 3 Comparison of future water stress projections of dynamic water stress for models with and without landscape heterogeneity, compiling dynamic water stress across 10 model runs, each forced with climate projections from 10 global climate models (GCMs) from 2006 to 2099, and two representative concentration pathways (RCP), 4.5 and 8.5

	Landscape heterogeneity	No landscape heterogeneity
RCP 4.5		
Dynamic water stress		
Mean	0.096	0.035
SD	0.079	0.058
Range	[0.000, 0.379]	[0.000, 0.367]
Landscape past threshold (%)		
Mean	5.5%	0.6%
SD	17.0%	8.0%
Range	[0%, 90.5%]	[0%, 100%]
No. of crossings at 100%	0	6
RCP 8.5		
Dynamic water stress		
Mean	0.104	0.038
SD	0.078	0.056
Range	[0.000, 0.362]	[0.000, 0.343]
Landscape past threshold (%)		
Mean	5.4%	0.2%
SD	16.2%	4.6%
Range	[0%, 90.0%]	[0%, 100%]
No. of crossings at 100%	0	2

projected future droughts are too severe and cause complete closure of stomata, then the benefit of elevated CO_2 will have no effect on photosynthesis (Franks *et al.*, 2013). Also, in some species, elevated CO_2 can cause changes in plant hydraulics that lead to greater potential for drought stress (Domec *et al.*, 2017). Although we found that stomatal conductance was linearly related to soil moisture (Fig. 3a), *J. ashei* showed a lagged recovery in gas exchange, despite an increase in rainfall during August (Johnson *et al.*, 2018b); our model does not account for delayed recovery from any hydraulic impairment. By not accounting for memory of impairment, we could be underestimating water stress, especially given the potential for consecutive droughts to increase in frequency with climate change. Lastly, models that can also account for re-growth/recovery of vegetation could provide additional insight on how landscape heterogeneity influences tree survival and recovery following drought (Tague *et al.*, 2013; Vicente-Serrano *et al.*, 2015).

Modeling future tree water stress

Using projected climate data from 10 global climate models (GCMs), we found that dynamic water stress was forecasted to increase through the 21st century due to both projected increases in PET and changes in the timing and amount of rainfall. Future projections of rainfall are highly uncertain; regional processes are often not included in many GCMs, causing projections of precipitation extremes to be less accurate at regional scales (Burke *et al.*, 2006; Jentsch *et al.*, 2007). However, there is high confidence in projected temperature increases; this warming also will lead to higher atmospheric moisture demand and PET (Fig. 7c). Higher projected PET values are likely the main driver of dynamic water stress increasing throughout the 21st century (Fig. 8a). When comparing models with and without landscape heterogeneity, it is important to consider that landscape heterogeneity allows for the existence of both stressful (e.g. drier, hotter) and favorable (e.g. wetter, cooler) landscape positions for tree growth. Not considering landscape heterogeneity results in the whole landscape experiencing the same level of water stress and requiring a more severe drought to cause stress. With landscape heterogeneity across a gradient of drought severity, some stress appears more readily, compared to the uniform landscape, (e.g. in hotter, drier landscape positions even under moderate drought). However, some refugia still remain under the most severe droughts. Therefore, when landscape heterogeneity is included, the range of water stress is lower due to buffering from cooler, mesic landscape positions during severe drought.

By including landscape heterogeneity in models, we identified microrefugia capable of buffering against water stress, allowing tree survival even during the most severe drought projected in the 21st century. For this study area, these microsites included areas with deep soil, substantial contributing area and northeastern-facing aspects. When considering outputs from 10 GCMs across the 21st century (2006–2099), the maximum percentage area of the watershed surpassing a dynamic water stress threshold associated with canopy loss was 100% for models with no landscape heterogeneity, compared to *c.* 90% for models including landscape heterogeneity (Table 3). For the most severe drought, only *c.* 10% of the landscape did not pass a dynamic water stress threshold associated with tree mortality in 2011. This supports the hypothesis of Allen *et al.* (2015) that the potential for microsites to buffer may be overwhelmed under the severe droughts and heatwaves projected under climate change. Alternatively, microsites might exist across the landscape that are too small to be adequately captured by the spatially distributed input variables of soil conditions and topography included in this model. For example, the SSURGO soil database does not identify areas with unique soil conditions below the minimum size map delineation of 0.4–4 ha. By using finer-scale digital elevation models (DEMs) and soil maps we could potentially identify additional microsites, capable of providing buffering against future water stress.

Failure to capture landscape heterogeneity in models could limit our capacity to accurately predict forest response to a changing climate. Tree mortality is often observed across local stress gradients within a species range, rather than at trailing range edges (Gitlin *et al.*, 2006). Therefore, when projecting future water stress, it is important to account for the fact that not all landscape positions are equally stressful. For our watershed in central Texas, models only predicted minimal buffering of tree water stress through the 21st century. However, different watersheds would likely have different buffering capacities, depending on the landscape complexity.

Models including landscape heterogeneity can also be used to determine the likely configuration of surviving stands. Landscape heterogeneity has the potential to act as a stabilizing process, if

seeds can disperse from surviving trees (Lloret *et al.*, 2012); these sites could then be prioritized for conservation (McLaughlin *et al.*, 2017). However, if droughts become too severe and leave only isolated stands, this isolation may limit dispersion and the potential for a species to migrate to keep pace with changing climate conditions (Hewitt & Kellman, 2004; Gitlin *et al.*, 2006; Lazarus & McGill, 2014).

Conclusion

We modeled dynamic water stress across a landscape at a 30-m spatial resolution by incorporating plant hydraulic thresholds in relation to water deficit and spatial heterogeneity of soil conditions (e.g. texture and depth), surface/subsurface lateral water flow using a topographic index, and PET attributable to radiation and temperature differences. Our model simplifies the plant hydraulics to maintain analytical tractability. As such, the model is currently computationally efficient to run at regional scales, while still accounting for local water stress gradients. Landscape heterogeneity typically is not considered in DGVMs, with coarse spatial resolutions of *c.* 10^4 to 10^5 km^2 (e.g. Moorcroft, 2006). Local water stress gradients with high spatial variability, combined with the nonlinear nature of mortality processes, suggest that modeling an average tree growing in an average environment will not give the same water stress predictions as a model that incorporates spatial heterogeneity of the environment (Levin *et al.*, 1997; Moorcroft, 2006). We found that including topographically variable input parameters improved our ability to predict spatial patterns of canopy loss observed during the 2011 drought. Furthermore, the model projected increases in mean dynamic water stress throughout the 21st century with the use of key physiological parameters of drought-induced vascular damage. Models with landscape heterogeneity showed some buffering capacity, but it was limited. The landscape can act as a buffer against water stress, but depending on the topography of the watershed, the buffering capacity has the potential to be overwhelmed if future droughts are too severe. By incorporating landscape heterogeneity in models, we can test whether landscapes can act as effective buffers against future droughts and heatwaves projected under climate change.

Acknowledgements

Our funding sources include a NASA Earth and Space Science Fellowship (NNX13AN86H), a James B. Duke Fellowship, a USDA National Institute of Food and Agriculture grant (2012-68002-19795), a National Science Foundation grant (NSF-IOS-1754893), and a NASA/AIST grant (AIST-16-0052). We also thank the Texas Parks and Wildlife Department for access to land for measuring LAI (permit no. 2016-0303).

Author contributions

A.M.S., A.J.P., N.P. and A.P. contributed to model development; A.M.S., D.M.J. and J-C.D. assisted with model parameterization; and A.M.S., A.J.P., J.J.S., D.M.J., J-C.D., R.B.J., N.P. and A.P. contributed to the design of the study and writing of the manuscript.

ORCID

Amanda M. Schwantes http://orcid.org/0000-0002-7791-1078
Anthony J. Parolari http://orcid.org/0000-0002-1046-6790
Daniel M. Johnson http://orcid.org/0000-0003-1015-9560
Jean-Christophe Domec http://orcid.org/0000-0003-0478-2559
Robert B. Jackson http://orcid.org/0000-0001-8846-7147
Amilcare Porporato http://orcid.org/0000-0001-9378-207X

References

Abatzoglou JT. 2013. Development of gridded surface meteorological data for ecological applications and modelling. *International Journal of Climatology* **33**: 121–131.

Abatzoglou JT, Brown TJ. 2012. A comparison of statistical downscaling methods suited for wildfire applications. *International Journal of Climatology* **32**: 772–780.

Adams HR, Barnard HR, Loomis AK. 2014. Topography alters tree growth – climate relationships in a semi-arid forested catchment. *Ecosphere* **5**: 1–16.

Adams HD, Williams AP, Xu C, Rauscher SA, Jiang X, McDowell NG. 2013. Empirical and process-based approaches to climate-induced forest mortality models. *Frontiers in Plant Science* **4**: 1–5.

Adams HD, Zeppel MJB, Anderegg WRL, Hartmann H, Landhäusser SM, Tissue DT, Huxman TE, Hudson PJ, Franz TE, Allen CD *et al.* 2017. A multi-species synthesis of physiological mechanisms in drought-induced tree mortality. *Nature Ecology & Evolution* **1**: 1285–1291.

Allen CD, Breshears DD, McDowell NG. 2015. On underestimation of global vulnerability to tree mortality and forest die-off from hotter drought in the Anthropocene. *Ecosphere* **6**: 1–55.

Allen CD, Macalady AK, Chenchouni H, Bachelet D, McDowell N, Vennetier M, Kitzberger T, Rigling A, Breshears DD, Hogg EH *et al.* 2010. A global overview of drought and heat-induced tree mortality reveals emerging climate change risks for forests. *Forest Ecology and Management* **259**: 660–684.

Allen RG, Pereira LS, Raes D, Smith M. 1998. *Crop evapotranspiration: guidelines for computing crop water requirements – FAO Irrigation and drainage paper 56.* Rome, Italy: Food and Agriculture Organization of the United Nations.

Anderegg WRL, Flint A, Huang C, Flint L, Berry JA, Davis FW, Sperry JS, Field CB. 2015. Tree mortality predicted from drought-induced vascular damage. *Nature Geoscience* **8**: 367–371.

Beven K. 1995. Linking parameters across scales: subgrid parameterizations and scale dependent hydrological models. *Hydrological Processes* **9**: 507–525.

Beven K. 1997. TOPMODEL: a critique. *Hydrological Processes* **11**: 1069–1085.

Beven KJ, Kirkby MJ. 1979. A physically based, variable contributing area model of basin hydrology. *Hydrological Sciences* **24**: 43–69.

Bowker MA, Muñoz A, Martinez T, Lau MK. 2012. Rare drought-induced mortality of juniper is enhanced by edaphic stressors and influenced by stand density. *Journal of Arid Environments* **76**: 9–16.

Brodribb TJ, Bowman DJMS, Nichols S, Delzon S, Burlett R. 2010. Xylem function and growth rate interact to determine recovery rates after exposure to extreme water deficit. *New Phytologist* **188**: 533–542.

Burke EJ, Brown SJ, Christidis N. 2006. Modeling the recent evolution of global drought and projections for the twenty-first century with the hadley centre climate model. *Journal of Hydrometeorology* **7**: 1113–1125.

Ciais P, Reichstein M, Viovy N, Granier A, Ogée J, Allard V, Aubinet M, Buchmann N, Bernhofer C, Carrara A *et al.* 2005. Europe-wide reduction in primary productivity caused by the heat and drought in 2003. *Nature* **437**: 529–533.

Clapp RB, Hornberger GM. 1978. Empirical equations for some soil hydrualic properties. *Water Resources Research* **14**: 601–604.

Clark JS, Iverson L, Woodall CW, Allen CD, Bell DM, Bragg DC, D'Amato AW, Davis FW, Hersh MH, Ibanez I *et al.* 2016. The impacts of increasing drought on forest dynamics, structure, and biodiversity in the United States. *Global Change Biology* **22**: 2329–2352.

Daly E, Oishi AC, Porporato A, Katul GG. 2008. A stochastic model for daily subsurface CO_2 concentration and related soil respiration. *Advances in Water Resources* **31**: 987–994.

Daly E, Porporato A, Rodriguez-Iturbe I. 2004. Coupled dynamics of photosynthesis, transpiration, and soil water balance. Part I: upscaling from hourly to daily level. *Journal of Hydrometeorology* **5**: 546–558.

Domec J-C, Gartner BL. 2001. Cavitation and water storage capacity in bole xylem segments of mature and young Douglas-fir trees. *Trees* **15**: 204–214.

Domec JC, Smith DD, McCulloh KA. 2017. A synthesis of the effects of atmospheric carbon dioxide enrichment on plant hydraulics: implications for whole-plant water use efficiency and resistance to drought. *Plant, Cell & Environment* **40**: 921–937.

Duan H, O'Grady AP, Duursma RA, Choat B, Huang G, Smith RA, Jiang Y, Tissue DT. 2015. Drought responses of two gymnosperm species with contrasting stomatal regulation strategies under elevated [CO_2] and temperature. *Tree Physiology* **35**: 756–770.

Dunne T, Moore TR, Taylor CH. 1975. Recognition and prediction of runoff-producing zones in humid regions. *Hydrological Sciences* **3**: 305–326.

Elliott LF, Diamond DD, True CD, Blodgett CF, Pursell D, German D, Treuer-Kuehn A. 2014. *Ecological mapping systems of Texas: summary report.* [WWW document] URL https://tpwd.texas.gov/landwater/land/programs/landscape-ecology/ems/[accessed 9 Jun 2014].

Engelbrecht BMJ, Comita LS, Condit R, Kursar TA, Tyree MT, Turner BL, Hubbell SP. 2007. Drought sensitivity shapes species distribution patterns in tropical forests. *Nature* **447**: 80–82.

Evans JS, Oakleaf J, Cushman SA, Theobald D. 2014. *An ArcGIS toolbox for surface gradient and geomorphometric modeling, version 2.0-0.* URL http://evansmurphy.wix.com/evansspatial [accessed 29 August 2017].

Fellows AW, Goulden ML. 2013. Controls on gross production by a semiarid forest growing near its warm and dry ecotonal limit. *Agricultural and Forest Meteorology* **169**: 51–60.

Feng X, Dawson TE, Ackerly DD, Santiago LS, Thompson SE. 2017. Reconciling seasonal hydraulic risk and plant water use through probabilistic soil–plant dynamics. *Global Change Biology* **23**: 3758–3769.

Franks PJ, Adams MA, Amthor JS, Barbour MM, Berry JA, Ellsworth DS, Farquhar GD, Ghannoum O, Lloyd J, McDowell N *et al.* 2013. Sensitivity of plants to changing atmospheric CO_2 concentration: from the geological past to the next century. *New Phytologist* **197**: 1077–1094.

Gitlin AR, Sthultz CM, Bowker MA, Stumpf S, Paxton KL, Kennedy K, Muñoz A, Bailey JK, Whitham TG. 2006. Mortality gradients within and among dominant plant populations as barometers of ecosystem change during extreme drought. *Conservation Biology* **20**: 1477–1486.

Hawthorne S, Miniat CF. 2017. Topography may mitigate drought effects on vegetation along a hillslope gradient. *Ecohydrology* **11**: e1825.

Heilman JL, Litvak ME, McInnes KJ, Kjelgaard JF, Kamps RH, Schwinning S. 2014. Water-storage capacity controls energy partitioning and water use in karst ecosystems on the Edwards Plateau, Texas. *Ecohydrology* **7**: 127–138.

Hewitt N, Kellman M. 2004. Factors influencing tree colonization in fragmented forests: an experimental study of introduced seeds and seedlings. *Forest Ecology and Management* **191**: 39–59.

Hoerling M, Kumar A, Dole R, Nielsen-Gammon JW, Eischeid J, Perlwitz J, Quan XW, Zhang T, Pegion P, Chen M. 2013. Anatomy of an extreme event. *Journal of Climate* **26**: 2811–2832.

Homer CG, Dewitz JA, Yang L, Jin S, Danielson P, Xian G, Coulston J, Herold ND, Wickham JD, Megown K. 2015. Completion of the 2011 National Land Cover Database for the conterminous United States-Representing a decade of land cover change information. *Photogrammetric Engineering and Remote Sensing* **81**: 345–354.

Hudson B. 1994. Soil organic matter and available water capacity. *Journal of Soil and Water Conservation* **49**: 189–194.

Jackson RB, Moore LA, Hoffmann WA, Pockman WT, Linder CR. 1999. Ecosystem rooting depth determined with caves and DNA. *Proceedings of the National Academy of Sciences, USA* **96**: 11387–11392.

Jackson RB, Randerson JT, Canadell JG, Anderson RG, Avissar R, Baldocchi DD, Bonan GB, Caldeira K, Diffenbaugh NS, Field CB *et al.* 2008. Protecting climate with forests. *Environmental Research Letters* **3**: 44 006.

Jentsch A, Kreyling J, Beierkuhnlein C. 2007. A new generation of climate-change experiments: events, not trends. *Frontiers in Ecology and the Environment* **5**: 365–374.

Johnson D, Berry Z, Baker K, Smith D, McCulloh K, Domec J-C. 2018a. Leaf hydraulic parameters are more plastic in species that experience a wider range of leaf water potentials. *Functional Ecology* **32**: 894–903.

Johnson DM, Domec J-C, Berry ZC, Schwantes AM, Woodruff DR, McCulloh KA, Wortemann R, Swenson JJ, Mackay DS, McDowell NG *et al.* 2018b. Co-occurring woody species have diverse hydraulic strategies and mortality rates during an extreme drought. *Plant Cell and Environment* **41**: 576–588.

Johnson DM, Wortemann R, McCulloh KA, Jordan-Meille L, Ward E, Warren JM, Palmroth S, Domec J-C. 2016. A test of the hydraulic vulnerability segmentation hypothesis in angiosperm and conifer tree species. *Tree physiology* **36**: 983–993.

Kaiser KE, McGlynn BL, Emanuel RE. 2013. Ecohydrology of an outbreak: mountain pine beetle impacts trees in drier landscape positions first. *Ecohydrology* **6**: 444–454.

Kavanagh KL, Bond BJ, Aitken SN, Gartner BL, Knowe S. 1999. Shoot and root vulnerability to xylem cabitation in four populations of Douglas-fir seedlings. *Tree Physiology* **19**: 31–37.

Kiniry JR. 1998. Biomass accumulation and radiation use efficiency of honey mesquite and eastern red cedar. *Biomass and Bioenergy* **15**: 467–473.

Korzukhin MD, Ter-Mikaelian MT, Wagner RG. 1996. Process versus empirical models: which approach for forest ecosystems management? *Canadian Journal of Forest Research* **26**: 879–887.

Laio F, Porporato A, Ridolfi L, Rodriguez-iturbe I. 2001. Plants in water-controlled ecosystems: active role in hydrologic processes and response to water stress II. Probalistic soil moisture dynamics. *Advances in Water Resources* **24**: 707–723.

Landsberg J. 1986. *Physiological ecology of forest production.* London, UK: Academic Press.

Lazarus ED, McGill BJ. 2014. Pushing the pace of tree species migration. *PLoS ONE* **9**: e105380.

Levin SA, Grenfell B, Hastings A, Perelson AS. 1997. Mathematical and computational challenges in population biology and ecosystems science. *Science* **275**: 334–343.

Lloret F, Escudero A, Iriondo JM, Martínez-Vilalta J, Valladares F. 2012. Extreme climatic events and vegetation: the role of stabilizing processes. *Global Change Biology* **18**: 797–805.

Loehle C, LeBlanc D. 1996. Model-based assessments of climate change effects on forests: a critical review. *Ecological Modelling* **90**: 1–31.

Lutz JA, van Wagtendonk JW, Franklin JF. 2010. Climatic water deficit, tree species ranges, and climate change in Yosemite National Park. *Journal of Biogeography* **37**: 936–950.

Mackay DS, Roberts DE, Ewers BE, Sperry JS, McDowell NG, Pockman WT. 2015. Interdependence of chronic hydraulic dysfunction and canopy processes can improve integrated models of tree response to drought. *Water Resources Research* **51**: 6156–6176.

McCune B, Keon D. 2002. Equations for potential annual direct incident radiation and heat load. *Journal of Vegetation Science* **13**: 603–606.

McDowell NG, Beerling DJ, Breshears DD, Fisher RA, Raffa KF, Stitt M. 2011. The interdependence of mechanisms underlying climate-driven vegetation mortality. *Trends in Ecology and Evolution* **26**: 523–532.

McDowell NG, Fisher RA, Xu C, Domec JC, Hölttä T, Mackay DS, Sperry JS, Boutz A, Dickman L, Gehres N *et al.* 2013. Evaluating theories of drought-induced vegetation mortality using a multimodel-experiment framework. *New Phytologist* **200**: 304–321.

McLaughlin BC, Ackerly DD, Klos PZ, Natali J, Dawson TE, Thompson SE. 2017. Hydrologic refugia, plants, and climate change. *Global Change Biology* **23**: 2941–2961.

Moorcroft PR. 2006. How close are we to a predictive science of the biosphere? *Trends in Ecology and Evolution* **21**: 400–407.

Moore ID, Burch GJ, Mackenzie DH. 1988. Topographic effects on the distribution of surface soil water and the location of ephemeral gullies. *Transactions of the ASAE* **31**: 1098–1107.

Moore GW, Edgar CB, Vogel JG, Washington-Allen RA, March RG, Zehnder R. 2016. Tree mortality from an exceptional drought spanning mesic to −semiarid ecoregions. *Ecological Applications* **26**: 602–611.

Moore ID, Grayson RB, Ladson AR. 1991. Digital terrain modeling: a review of hydrological geomorphological and biological applications. *Hydrological Processes* **5**: 3–30.

Mueller RC, Scudder CM, Porter ME, Trotter RT, Gehring CA, Whitham TG. 2005. Differential tree mortality in response to severe drought: evidence for long-term vegetation shifts. *Journal of Ecology* **93**: 1085–1093.

Norman JM, Campbell GS. 1989. Canopy structure. In: Pearcy RW, Ehleringer J, Mooney HA, Rundel PW, eds. *Plant physiological ecology: field methods and instrumentation*. New York, NY, USA: Chapman and Hall, 301–325.

Owens MK, Lyons RK, Alejandro CL. 2006. Rainfall partitioning within semiarid juniper communities: effects of event size and canopy cover. *Hydrological Processes* **20**: 3179–3189.

Parolari AJ, Katul GG, Porporato A. 2014. An ecohydrological perspective on drought-induced forest mortality. *Journal of Geophysical Research: Biogeosciences* **119**: 965–981.

Pellenq J, Kalma J, Boulet G, Saulnier GM, Wooldridge S, Kerr Y, Chehbouni A. 2003. A disaggregation scheme for soil moisture based on topography and soil depth. *Journal of Hydrology* **276**: 112–127.

Peterman W, Waring RH. 2014. Does overshoot in leaf development of ponderosa pine in wet years leads to bark beetle outbreaks on fine-textured soils in drier years? *Forest Ecosystems* **1**: 24.

Plaut JA, Yepez EA, Hill J, Pangle R, Sperry JS, Pockman WT, Mcdowell NG. 2012. Hydraulic limits preceding mortality in a piñon–juniper woodland under experimental drought. *Plant, Cell & Environment* **35**: 1601–1617.

Porporato A, Laio F, Ridolfi L, Rodriguez-Iturbe I. 2001. Plants in water-controlled ecosystems: active role in hydrologic processes and response to water stress: III. Vegetation water stress. *Advances in Water Resources* **24**: 725–744.

Quinn P, Beven K, Culf A. 1995. The introduction of macroscale hydrological complexity into land surface-atmosphere transfer models and the effect on planetary boundary layer development. *Journal of hydrology* **166**: 421–444.

Rodriguez-Iturbe I, Porporato A. 2004. *Ecohydrology of water-controlled ecosystems*. Cambridge, UK: Cambridge University Press.

Rodriguez-Iturbe I, Porporato A, Ridolfi L, Isham V, Cox DR. 1999. Probabilistic modelling of water balance at a point: the role of climate soil and vegetation. *Proceedings of the Royal Society A* **455**: 3789–3805.

Schwantes AM, Swenson JJ, González-Roglich M, Johnson DM, Domec J-C, Jackson RB. 2017. Measuring canopy loss and climatic thresholds from an extreme drought along a fivefold precipitation gradient across Texas. *Global Change Biology* **23**: 5120–5135.

Schwantes AM, Swenson JJ, Jackson RB. 2016. Quantifying drought-induced tree mortality in the open canopy woodlands of central Texas. *Remote Sensing of Environment* **181**: 54–64.

Sing T, Sander O, Beerenwinkel N, Lengauer T. 2005. ROCR: visualizing classifier performance in R. *BioInfomatics* **21**: 3940–3941.

Sperry JS, Adler FR, Campbell GS, Comstock JP. 1998. Limitation of plant water use by rhizosphere and xylem conductance: results from a model. *Plant, Cell & Environment* **21**: 347–359.

Sperry JS, Love DM. 2015. What plant hydraulics can tell us about responses to climate-change droughts. *New Phytologist* **207**: 14–27.

Tague CL, McDowell NG, Allen CD. 2013. An integrated model of environmental effects on growth, carbohydrate balance, and mortality of Pinus ponderosa forests in the southern Rocky Mountains. *PLoS ONE* **8**: e80286.

Tai X, Mackay DS, Anderegg WRL, Sperry JS, Brooks PD. 2017. Plant hydraulics improves and topography mediates prediction of aspen mortality in southwestern USA. *New Phytologist* **213**: 113–127.

Tarboton DG. 2005. *Terrain analysis using digital elevation models (TauDEM)*. [WWW document] URL http://hydrology.usu.edu/taudem/taudem5/index.html [accessed 3 November 2015].

Twidwell D, Wonkka CL, Taylor CA, Zou CB, Twidwell JJ, Rogers WE. 2014. Drought-induced woody plant mortality in an encroached semi-arid savanna depends on topoedaphic factors and land management. *Applied Vegetation Science* **17**: 42–52.

Tyree MT, Ewers FW. 1991. The hydraulic architecture of trees and other woody plants. *New Phytologist* **119**: 345–360.

United States Department of Agriculture. 2014. *Soil survey staff, Natural Resources Conservation Service. Soil Survey Geographic (SSURGO) Database*. [WWW document] URL https://gdg.sc.egov.usda.gov/[accessed 29 August 2017].

Vicente-Serrano SM, Camarero JJ, Zabalza J, Sangüesa-Barreda G, López-Morenoa JI, Tague CL. 2015. Evapotranspiration deficit controls net primary production and growth of silver fir: Implications for Circum-Mediterranean forests under forecasted warmer and drier conditions. *Agricultural and Forest Meteorology* **206**: 45–54.

Vicente-Serrano SM, Lopez-Moreno J-I, Beguería S, Lorenzo-Lacruz J, Sanchez-Lorenzo A, García-Ruiz JM, Azorin-Molina C, Morán-Tejeda E, Revuelto J, Trigo R *et al.* 2014. Evidence of increasing drought severity caused by temperature rise in southern Europe. *Environmental Research Letters* **9**: 44 001.

Viola F, Daly E, Vico G, Cannarozzo M, Porporato A. 2008. Transient soil-moisture dynamics and climate change in Mediterranean ecosystems. *Water Resources Research* **44**: 1–12.

Western AW, Grayson RB, Blöschl G, Willgoose GR. 1999. Observed spatial organization of soil moisture and its relation to terrain indices. *Water Resources Research* **35**: 797–810.

Willson CJ, Manos PS, Jackson RB. 2008. Hydraulic traits are influenced by phylogenetic history in the drought-resistant, invasive genus Juniperus (Cupressaceae). *American Journal of Botany* **95**: 299–314.

Wolock DM, Price CV. 1994. Effects of digital elevation model map scale and data resolution on a topography-based watershed model. *Water Resources Research* **30**: 3041–3052.

Zhu AX, Mackay DS. 2001. Effects of spatial detail of soil information on watershed modeling. *Journal of Hydrology* **248**: 54–77.

Supporting Information

Additional Supporting Information may be found online in the Supporting Information section at the end of the article:

Fig. S1 Accuracy in distinguishing drought-impacted stands from homogenous live canopy stands of *J. ashei* above a certain size threshold up to 60 ha.

Table S1 Comparison of accuracy in distinguishing drought-impacted vs live stands using multiple values for the parameter controlling incipient stomatal closure

Table S2 Comparison of 20 GCMs in predicting annual rainfall from 1980 to 2005 for the study watershed

Methods S1 Analytical solutions for static water stress and crossing properties.

Methods S2 Further justification for selecting incipient and complete stomatal closure parameters.

Please note: Wiley Blackwell are not responsible for the content or functionality of any Supporting Information supplied by the authors. Any queries (other than missing material) should be directed to the *New Phytologist* Central Office.